PHYSICAL REVIEW B **74**, 235414 (2006)

Ground states of diatomic molecules adsorbed on single-walled carbon nanotubes

Yi Ding and Jun Ni

Department of Physics and Key Laboratory of Atomic and Molecular Nanoscience (Ministry of Education), Tsinghua University, Beijing 100084, People's Republic of China

(Received 26 April 2006; revised manuscript received 8 October 2006; published 8 December 2006)

We have studied the adsorption of diatomic molecules on graphite sheets and carbon nanotubes using Monte Carlo simulations. We have obtained the ground states for two-site dimer adsorption. On the high-coverage side, the ground states for dimer adsorption are highly degenerate. The complementary vacancy structures and the variation tendency of the ordered structures with increase of nanotube size are similar to those for single-site adsorption. On the low-coverage side, most dimer ordered structures are not degenerate. The confinement of nanotubes leads to helical ground-state structures for dimer adsorption.

DOI: 10.1103/PhysRevB.74.235414 PACS number(s): 68.43.De, 68.43.Fg, 61.46.−w

I. INTRODUCTION

Atom and molecule adsorption on nanotubes has attracted much experimental and theoretical attention because of its scientific interest and potential technological applications.[1–11] Adsorption on carbon nanotubes affects the electronic conductance of nanotubes[12–16] and has the potential of revolutionizing gas storage technology.[17–20]

A single-walled carbon nanotube (SWNT) can be considered as a rolled graphite sheet. Extensive research has been carried out to investigate the interaction between adsorbates and the graphite.[21–23] It is found that the stable positions of alkali-metal adatoms are on the centers of the graphite hexagons.[22] The preferred adsorption sites for H_2 and N_2 molecules are also on the centers of the graphite hexagons.[23] For adsorption on carbon nanotubes, the center of each carbon hexagon is still considered as a preferred adsorption site. First-principle calculations show that the centers of the carbon hexagons of SWNTs are the optimal sites for gas molecules such as H_2, N_2, and Ar[1,2] and for most metal atoms.[24] A triangular lattice gas model has been used to describe the behavior of submonolayers of adsorbates on graphite with the centers of carbon hexagons as adsorption sites.[25] The corresponding possible ground-state structures have been investigated using various methods.[26,27] When graphite is rolled into nanotubes, the effects of size confinement on the ground-state structures have been studied by the Monte Carlo method.[28]

Most of the studies on surface adsorption are devoted to adsorption with single occupancy. For the adsorption of molecules on graphite and nanotubes, there are two cases: one is the adsorption of small molecules such as H_2, for which the whole adsorbed molecule is localized in the carbon hexagons; while for the adsorption of large molecules, one adsorbed molecule may occupy several lattice sites. When Br_2 molecules are adsorbed on graphite, each Br atom of a diatomic molecule occupies the center of a carbon hexagon and a Br_2 molecule occupies two neighboring sites.[29,30] Compared with single-site adsorption, multisite adsorption is more complex. There is no statistical equivalence between adsorbates and vacancies. The phase diagrams are thus not symmetrical around coverage $\theta=1/2$ like those of the single-site adsorption. An isolated vacancy cannot serve to adsorb molecules and the occupation of a given lattice site demands that at least one of its neighboring sites is also occupied. In addition, the effect of size confinement in adsorption on nanotubes becomes stronger due to difficulties in multisite matching with these constraints.

In this paper, we study the two-site adsorption of diatomic molecules on graphite and carbon nanotubes. We show the results for ground-state structures of diatomic molecules on graphite and carbon nanotubes. We also give an analysis of the distinct features of the ground states of the two-site adsorption. In Sec. II we describe the model and methods. In Sec. III we present the results and discussion. Section IV is the summary.

II. METHOD

We consider the adsorption of large diatomic molecules such as Br_2 on graphite and carbon nanotubes, a two-site adsorption situation. The adsorption sites on the centers of carbon hexagons of the graphite sheet form a two-dimensional triangular lattice. The adsorbed diatomic molecules are modeled as dimers, which occupy two neighboring lattice sites.[31–33] When a graphite sheet is rolled into a nanotube, the system is confined in the rolling direction. The lattice of the adsorption sites on a carbon nanotube is periodic along the rolling direction. Similar to diatomic molecule adsorption on graphite, we use the dimer model to describe adsorbed diatomic molecules on nanotubes. The difference of adsorption on nanotubes from that on graphite is that lattices for nanotubes are periodic along the rolling direction, which leads to additional frustration effects and size confinement in adsorbate structures.[28]

In order to describe the ordered structures of adsorbed dimers, we introduce the spin variable s_i. s_i is equal to 1 when the corresponding site i is occupied by a dimer. Otherwise, s_i is equal to −1. The Hamiltonian of the system is given as

$$H = J_1 \sum_{NN} s_i s_j + J_2 \sum_{NNN} s_i s_j + \mu \sum_i s_i - N J_1,$$

where J_1 is the nearest-neighbor interaction, J_2 is the next-nearest-neighbor interaction, and μ is the chemical potential. The first sum runs over all the nearest-neighbor site pairs, the

©2006 The American Physical Society

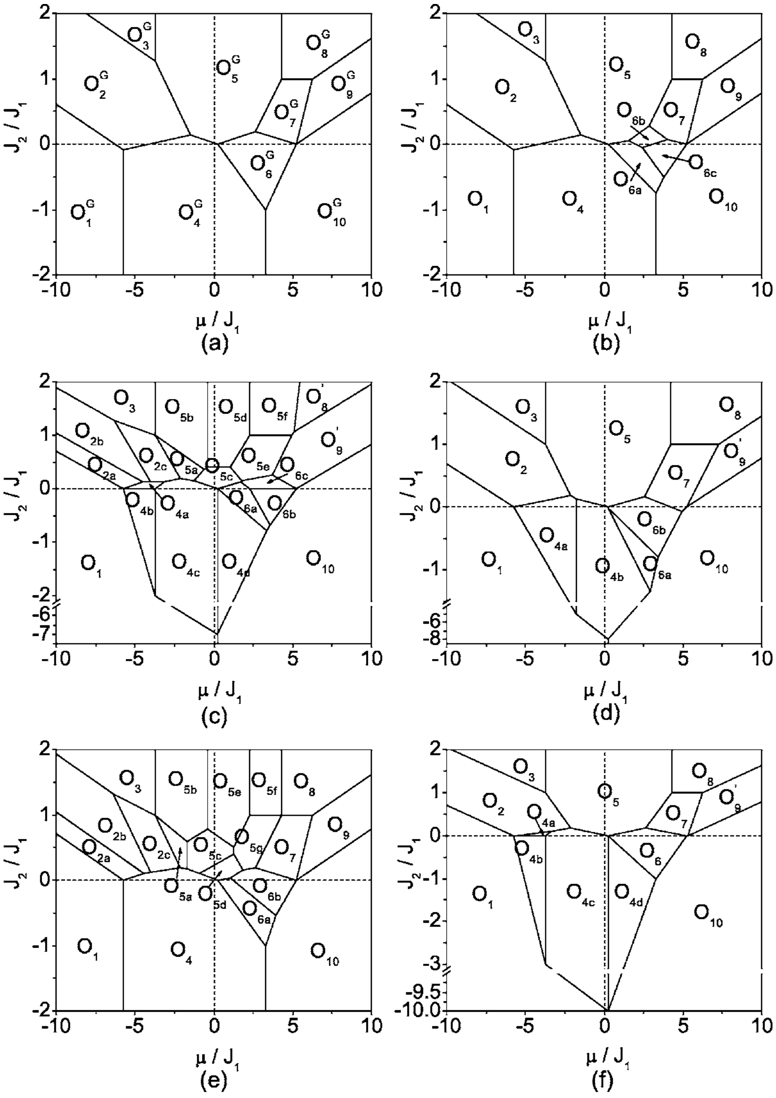

FIG. 1. Ground-state phase diagrams for dimer adsorption on (a) graphite, (b) (6,0) nanotube, (c) (7,0) nanotube, (d) (8,0) nanotube, (e) (9,0) nanotube, and (f) (10,0) nanotube.

second sum runs over all the next-nearest-neighbor site pairs, and the last sum runs over all the sites. N is the number of adsorbed dimers. The term NJ_1 is subtracted in the Hamiltonian since the summation over all the nearest-neighbor site pairs overestimates the total energy by including N bonds belonging to the N adsorbed dimers.[31–33]

We use Monte Carlo simulation to find all the possible ground states of the system.[34] In the calculations, we allow the system to anneal down from the state at high temperature to an ordered state at low temperature. During the process of annealing, there are three basic movements: adsorption, desorption, and rotation of an adsorbed dimer.[35] When the temperature approaches zero, the system will be annealed into the ground state. In order to obtain all possible ground states, we scan the parameter space of the chemical potential and the interaction energies. In order to describe diatomic molecule adsorption, such as adsorbed Br_2 on graphite and carbon nanotubes, we consider the nearest-neighbor interaction as repulsive.[29,30] J_1 is set as a renormalization parameter and we consider the parameter space of μ/J_1 and J_2/J_1.

III. RESULTS

In order to obtain the possible ground states of adsorbed dimers on graphite, we use a triangular 60×60 lattice with periodic boundary condition in the calculations. We find ten different types of ground states for dimer adsorption on graphite. The corresponding phase diagram of ground states is shown in Fig. 1(a). The structures of the ground states are shown in Fig. 2. The coverage θ is defined as $2N/M$, where N is the number of adsorbed dimers and M is the number of lattice sites. The factor of 2 is because one dimer occupies two neighboring lattice sites. González *et al.* considered the nearest-neighbor interaction to study dimer adsorption on a triangular lattice.[31] We obtain the same structures (the O_4^G and O_6^G phases) as theirs at the coverages $\theta=2/3$ and $2/5$. We find the O_2^G ($\theta=3/4$) phase at high coverage in addition to the O_4^G and O_6^G phases for dimer adsorption with nearest-neighbor interaction. Compared with single-site adsorption, we get more complex structures. It is found that there are nine different ground states for single-site adsorption with a repulsive nearest-neighbor interaction $J_1>0$,[28] fewer than for dimer adsorption.

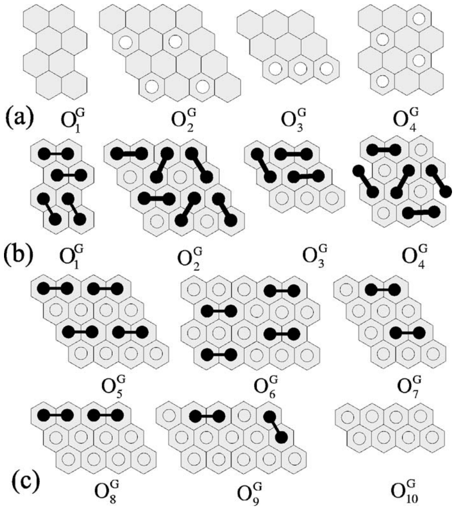

FIG. 2. (a) Vacancy-ordered structures of the O_1^G, O_2^G, O_3^G, and O_4^G phases with coverage $\theta > 1/2$. The white circles represent vacancies. The other hexagon centers are occupied by dimers. (b) Examples of dimer coverings of the O_1^G, O_2^G, O_3^G, and O_4^G phases. Black circles joined by black lines represent adsorbed dimers, and hollow circles represent vacancies. (c) Ground-state structures of dimer adsorbates on the graphite with coverage $\theta \leqslant 1/2$.

In dimer adsorption, due to possible orientations of dimers, the primitive cells of ground states of adsorbates on the graphite are complex and have large size. In particular, the O_1^G, O_2^G, O_3^G, and O_4^G phases with high coverage $\theta > 1/2$ are highly degenerate due to the possibility of different dimer coverings on the occupied sites. From our calculations we find that these highly degenerate phases with $\theta > 1/2$ can be characterized by the complementary vacancy ordered structures. Figure 2(a) shows vacancy ordered structures of the O_1^G, O_2^G, O_3^G, and O_4^G phases. The structure of the O_1^G (θ=1) phase is the full occupied structure. When we consider the ordered structures formed by vacancies, the corresponding complementary vacancy structure of the O_2^G (θ=3/4) phase is the same as the 2×2 ordered structure.[28] The corresponding complementary vacancy structure of the O_3^G (θ=2/3) phase is the same as the 3×1 ordered structure of single-site adsorption. The corresponding complementary vacancy structure of the O_4^G (θ=2/3) phase is the same as the $\sqrt{3} \times \sqrt{3}$ ordered structure of single-site adsorption. Due to the possible orientations of dimers, there are a lot of different dimer coverings for the O_1^G (θ=1), O_2^G (θ=3/4), O_3^G (θ=2/3), and O_4^G (θ=2/3) phases, leading to highly degenerate ground-state structures. Figure 2(b) shows examples of dimer coverings for each of these degenerate ground states. For the low-coverage phases with $\theta \leqslant 1/2$, we will consider the dimer ordered structures directly. The structure of the O_5^G (θ=1/2) phase is similar to the $\sqrt{3} \times 1$ ordered structure of single-site adsorption, in which the dimers are along the parallel lines. The structure of the O_8^G (θ=1/3) phase is similar to the 3×1 ordered structure of single-site adsorption. The O_8^G (θ=1/3) phase has three orientation variants, due to the three equivalent orientations in the triangular lattice. The structure of the O_{10}^G (θ=0) phase is the vacant structure. The structures of the O_6^G (θ=2/5), the O_9^G (θ=4/15), and the O_7^G (θ=1/3) phases have no corresponding ordered structures of single-site adsorption.

Now we show the results for the ground states of diatomic molecule adsorbates on $(n,0)$ zigzag nanotubes. We denote as l the number of lattice sites along the axis of the nanotubes, which will be taken large enough for end effects to be neglected. We take l=60 and use periodic boundary conditions. Calculations on other geometries such as l=90 and 120 are also performed and the same results are obtained. We have calculated the cases of n=6–10 and shown that the ground states of dimer adsorption are much complex than those of single-site adsorption. Since the symmetries of nanotubes can be described with the line groups,[36,37] which contain all symmetries of systems periodic in one direction,[38] we use the line groups and coverages to characterize the ground states. The line group $\mathbf{L}$ can be a product $\mathbf{L}=\mathbf{ZP}$ of one axial point group $\mathbf{P}$ and one infinite cyclic group $\mathbf{Z}$, and this factorization uniquely defines 13 line group families.[36–38] By the elements $(P|t)$ of line group $\mathbf{L}$ we mean that $(P|t)$: $(\rho,\phi,z) \rightarrow (\rho,\phi',z+ta)$ in cylindrical coordinates, where a is the length of the primitive cell along the axis. We list all the international symbols for line groups for dimer adsorption on $(n,0)$ nanotubes in Table I. The coverage θ of the O_{10} phase is zero and thus the line group of the O_{10} phase is the same as that of the pristine $(n,0)$ nanotube. We have also used the structure factor $S(k)$ to characterize the ordered phases. The structure factor $S(\mathbf{k})$ of the system is defined as $S(\mathbf{k})=\langle \rho(\mathbf{k})\rho(-\mathbf{k})\rangle / M$, where $\rho(\mathbf{k})=\Sigma_i s_i \exp(i\mathbf{k}\cdot\mathbf{r}_i)$ and M is the number of lattice sites.[39–41] For $(n,0)$ nanotubes, the wave vectors associated with the rolling direction need to be quantized, while the wave vectors associated with the axis direction remain continuous. So $\mathbf{k}=k\mathbf{K}_2/|\mathbf{K}_2|+\mu\mathbf{K}_1$, where μ is an integer between 0 and $2n$.[42] In Table II, we list the expressions for $S(k)$ for dimer adsorption on $(n,0)$ nanotubes in the case of μ =0. The structure factor $S(k)$ of the system is the fourier transform of the two-point correlation function,[34] which depends on the ground state of the adsorbed structures. So $S(k)$ can be used as a kind of order parameter to identify each phase. In order to describe the variation of the structures on the nanotubes, we consider the primitive cells of the O_i^G phases as the basic substructures of the corresponding phases on the nanotubes and the primitive cells of complementary vacancy ordered structures of the O_i^G phases with $\theta > 1/2$ as the basic vacancy substructures of the corresponding phases on the nanotubes.

In the case of n=6, there are 12 ground states of dimer adsorbates. The phase diagram is shown in Fig. 1(b). The structures of the different ground states as compared with the structures on graphite are shown in Fig. 3. The others are constructed using the same repeating structure units as those in Fig. 2 and keep most of the symmetries of the (6,0) nanotube as shown in Table I. There are three different ground states O_{6a} (θ=4/9), O_{6b} (θ=7/18), and O_{6c} (θ=10/27) derived from the O_6^G (θ=2/5) phase of adsorbed dimers on the graphite. The derived O_{6i} ($i=a,b,c$) phases have H-shape structures composed of two parallel dimers and a vacancy, similar to that of the O_6^G (θ=2/5) phase on graphite. The O_{6c} (θ=10/27) phase is a helical structure along the nanotube,

TABLE I. Line groups for the ground-state phases of dimers adsorbed on $(n,0)$ nanotubes.

n=6		n=7		n=8		n=9		n=10	
Phase	Line group	Phase	Line group	Phase	Line group	Phase	Line group	Phase	Line group
O_1	$L12_6/mcm$	O_1	$L14_7/mcm$	O_1	$L16_8/mcm$	O_1	$L18_9/mcm$	O_1	$L20_{10}/mcm$
O_2	$L6_3/mcm$	O_{2a}	$L\bar{2}2c$	O_2	$L8_4/mcm$	O_{2a}	$L\bar{2}2c$	O_2	$L10_5/mcm$
O_3	$L12_6/mcm$	O_{2b}	$L\bar{2}2m$	O_3	$L16_8/mcm$	O_{2b}	$L\bar{2}2m$	O_3	$L20_{10}/mcm$
O_4	$L4_2/mcm$	O_{2c}	$L\bar{2}2c$	O_{4a}	$L\bar{1}m$	O_{2c}	$L\bar{2}2c$	O_{4a}	$L20_72$
O_5	$L6/mmm$	O_3	$L14_7/mcm$	O_{4b}	$L16_82$	O_3	$L18_9/mcm$	O_{4b}	$L\bar{2}2c$
O_{6a}	$L2/mcc$	O_{4a}	$L14_52$	O_5	$L8/mmm$	O_4	$L6_3/mcm$	O_{4c}	$L\bar{2}2m$
O_{6b}	$L\bar{1}m$	O_{4b}	$L\bar{2}2c$	O_{6a}	$L8_32$	O_{5a}	$L\bar{2}2m$	O_{4d}	$L\bar{2}2m$
O_{6c}	$L4_12$	O_{4c}	$L\bar{2}2m$	O_{6b}	$L16_12$	O_{5b}	$L18_{11}2$	O_5	$L10/mmm$
O_7	$L6_222$	O_{4d}	$L\bar{2}2m$	O_7	$L16_{12}22$	O_{5c}	$L1_12$	O_6	$L4_2/mcm$
O_8	$L12_6/mcm$	O_{5a}	$L\bar{2}2m$	O_8	$L16_8/mcm$	O_{5d}	$L\bar{2}2m$	O_7	$L20_{15}2$
O_9	$L2/mcc$	O_{5b}	$L14_32$	O_9'	$L16_82$	O_{5e}	$L9_5$	O_8	$L20_{10}/mcm$
O_{10}	$L12_6/mcm$	O_{5c}	$L\bar{2}2c$	O_{10}	$L16_8/mcm$	O_{5f}	$L18_12$	O_9'	$L\bar{4}2c$
		O_{5d}	$L7_4$			O_{5g}	$L1m$	O_{10}	$L20_{10}/mcm$
		O_{5e}	$L7_12$			O_{6a}	$L1/m$		
		O_{5f}	$L14_12$			O_{6b}	$L9_1$		
		O_{6a}	$L7_42$			O_7	$L9_32$		
		O_{6b}	$L\bar{2}2c$			O_8'	$L18_32$		
		O_{6c}	$L14_12$			O_9	$L\bar{6}2c$		
		O_8'	$L\bar{2}2m$			O_{10}	$L18_9/mcm$		
		O_9'	$L1c$						
		O_{10}	$L14_7/mcm$						

whose main part is constructed with the basic substructure of the O_6^G (θ=2/5) phase. The structure in the dashed rectangle of Fig. 3 is the repeating helical unit of the O_{6c} (θ=10/27) phase. When the nanotube unwinds to a graphite sheet, the helical direction and the axis of the nanotube form an angle α with $\tan\alpha=\sqrt{3}/9$ shown in Fig. 3. According to the line groups, the generator of the translational subgroup is different for these three phases: for the O_{6a} (θ=4/9) phase it is $(\sigma_v|\frac{1}{2})$, for the O_{6b} (θ=7/18) phase it is $(E|1)$, and for the O_{6c} (θ=10/27) phase it is $(C_4^1|\frac{1}{4})$. The structure of O_9 (θ=4/15) is composed of the corresponding basic substructures plus their mirror reflections, which causes a lower symmetry of the line group.

In the case of n=7, there are 21 ground states of dimer adsorbates. The phase diagram is shown in Fig. 1(c). The structures of the different phases are shown in Fig. 4, and the others are constructed using the same repeating structure units as those in Fig. 2. On the (7,0) nanotube, the O_6^G (θ=2/5) phase is split into three phases O_{6a} (θ=3/7), O_{6b} (θ=8/21), and O_{6c} (θ=8/21). For the O_{6b} (θ=8/21) phase, the basic substructure of the O_6^G (θ=2/5) phase is its main part. For the O_{6a} (θ=3/7) and O_{6c} (θ=8/21) phases, the basic substructure of the O_6^G (θ=2/5) phase is arranged helically on the (7,0) nanotube. The helical direction of the O_{6a} (θ=3/7) phase and the axis of the (7,0) nanotube form an angle α with $\tan\alpha=2\sqrt{3}/3$. For the helical direction of the O_{6c} (θ=8/21) phase, we have $\tan\alpha=\sqrt{3}/9$. On the (7,0) nanotube, the O_4^G (θ=2/3) phase is split into four phases O_{4a} (θ=5/7), O_{4b} (θ=5/7), O_{4c} (θ=9/14), and O_{4d} (θ=4/7). The structures of the O_{4b} (θ=5/7), O_{4c} (θ=9/14), and O_{4d} (θ=4/7) phases are derived from the O_4^G (θ=2/3) phase due to the confinement in the rolling direction. The vacancies of the O_{4a} (θ=5/7) phase form a helical line surrounding the nanotube. The helical line and the axis of the (7,0) nanotube form an angle α with $\tan\alpha=\sqrt{3}$. The O_2^G (θ=3/4) phase is split into three phases O_{2a} (θ=11/14), O_{2b} (θ=3/4), and O_{2c} (θ=5/7) due to the confinement in the rolling direction. The O_5^G (θ=1/2) phase is split into six phases O_{5a} (θ=4/7), O_{5b} (θ=19/35), O_{5c} (θ=1/2), O_{5d} (θ=1/2), O_{5e} (θ=3/7), and O_{5f} (θ=3/7). In the structures of the O_{5b} (θ=19/35), O_{5d} (θ=1/2), O_{5e} (θ=3/7), and O_{5f} (θ=3/7) phases, most dimers are arrange helically to form helical units. The helical direction of these four phases and the axis of the (7,0) nanotube form an angle α with $\tan\alpha=\sqrt{3}/3$. The O_8' (θ=22/63) and O_9' (θ=6/21) phases are derived from the corresponding O_8^G (θ=1/3) and O_9^G (θ=4/15) phases due to the confinement in the rolling direction. Since the (7,0) nanotube is not compatible with those basic substructures as discussed in the following in detail, the symmetries of most phases are low as shown in Table I for the case of n=7.

In the case of n=8, there are 12 ground states of dimer adsorbates. The phase diagram is shown in Fig. 1(d). The

TABLE II. $S(k)$ for the ground-state phases of dimers adsorbed on $(n,0)$ nanotubes.

Phase	$S(k)$	Phase	$S(k)$
	$n=6$		$n=7$
O_1	$12\cos(k\pi)^2$	O_1	$14\cos(k\pi)^2$
O_2	$6\cos(2k\pi)^2$	O_{2a}	$\frac{2}{7}\cos(2k\pi)^2[25+7\cos(2k\pi)]$
O_3	$-4\cos(3k\pi)^2[2\cos(4k\pi)-3]$	O_{2b}	$\frac{1}{14}[50+7\cos(2k\pi)+48\cos(4k\pi)-7\cos(6k\pi)]$
O_4	$\frac{4}{3}\cos(k\pi)^2$	O_{2c}	$-\frac{2}{7}\cos(2k\pi)^2[7\cos(2k\pi)-25]$
O_5	$12\sin(k\pi)^2$	O_3	$-\frac{14}{3}\cos(3k\pi)^2[2\cos(4k\pi)-3]$
O_{6a}	$\frac{4}{9}\cos(k\pi)^2[1-2\cos(2k\pi)]^2$	O_{4a}	$\frac{18}{14}(\Sigma_{n=0}^{6}\cos[(2n+1)k\pi])^2$
O_{6b}	$\frac{2}{9}[1-2\cos(2k\pi)]^2[3+3\cos(2k\pi)+2\cos(4k\pi)]$	O_{4b}	$\frac{18}{7}\cos(k\pi)^2$
O_{6c}	$\frac{4}{81}(\Sigma_{n=0}^{2}\cos[9k(2n+1)\pi])^2[11+2\cos(2k\pi)+12\cos(4k\pi)$ $+8\cos(6k\pi)\quad+2\cos(8k\pi)+10\cos(10k\pi)+4\cos(14k\pi)]$	O_{4c}	$\frac{1}{7}[5+3\cos(2k\pi)]$
O_7	$-\frac{2}{9}[3\cos(2k\pi)-5][1+2\cos(4k\pi)]^2$	O_{4d}	$\frac{2}{7}\cos(k\pi)^2$
O_8	$-4\cos(3k\pi)^2[2\cos(4k\pi)-3]$	O_{5a}	$\frac{1}{7}\cos(4k\pi)^2[78-91\cos(2k\pi)+70\cos(4k\pi)-49\cos(6k\pi)]$
O_9	$\frac{4}{15}\cos(5k\pi)^2[21+8\cos(2k\pi)+10\cos(4k\pi)+16\cos(6k\pi)$ $-6\cos(8k\pi)]$	O_{5b}	$-\frac{1}{245}(1+2\Sigma_{n=1}^{3}\cos(10nk\pi))^2[8\cos(2k\pi)-2\cos(4k\pi)$ $-8\cos(6k\pi)\quad+6\cos(8k\pi)-13]$
O_{10}	$12\cos(k\pi)^2$	O_{5c}	$\frac{25}{14}(\Sigma_{n=0}^{3}(-1)^n\sin((2n+1)k\pi))^2$
	$n=8$	O_{5d}	$\frac{1}{49}(\Sigma_{n=0}^{13}(-1)^n\sin[(2n+1)k\pi])^2$
O_1	$16\cos(k\pi)^2$	O_{5e}	$\frac{2}{49}(\Sigma_{n=0}^{6}\cos[(2n+1)k\pi])^2$
O_2	$8\cos(2k\pi)^2$	O_{5f}	$\frac{2}{49}(\Sigma_{n=0}^{6}\cos[(2n+1)k\pi])^2$
O_3	$-\frac{16}{3}\cos(3k\pi)^2[2\cos(4k\pi)-3]$	O_{6a}	$\frac{2}{49}(\Sigma_{n=0}^{6}\cos[(2n+1)k\pi])^2$
O_{4a}	$\frac{5}{4}+\cos(2k\pi)$	O_{6b}	$\frac{2}{21}\cos(3k\pi)^2[11+8\cos(2k\pi)+6\cos(4k\pi)]$
O_{4b}	$\cos(k\pi)^2$	O_{6c}	$\frac{2}{147}(\Sigma_{n=0}^{20}\cos[(2n+1)k\pi]+2\Sigma_{n=1}^{13}\cos(3nk\pi))^2$
O_5	$16\sin(k\pi)^2$	O_8'	$-\frac{2}{63}\cos(9k\pi)^2[140\cos(2k\pi)+226\cos(4k\pi)$ $-448\cos(6k\pi)\ +118\cos(8k\pi)+112\cos(10k\pi)$ $-266\cos(12k\pi)+28\cos(14k\pi)\ +98\cos(16k\pi)-369]$
O_{6a}	0	O_9'	$\frac{2}{21}\cos(3k\pi)^2[51+16\cos(2k\pi)+14\cos(4k\pi)]$
O_{6b}	$\frac{2}{3}\cos(2k\pi)^4(\Sigma_{n=0}^{1}\{\cos[(24n+5)k\pi]-\cos[(24n+9)k\pi]$ $+\cos[(24n+11)k\pi]+\cos[(24n+13)k\pi]$ $-\cos[(24n+15)k\pi]+\cos[(24n+19)k\pi]\})$	O_{10}	$14\cos(k\pi)^2$

TABLE II. (*Continued.*)

Phase	$S(k)$
O_7	$\frac{8}{3}[\cos(3k\pi)+\cos(9k\pi)]^2$
O_8	$-\frac{16}{3}\cos(3k\pi)^2[2\cos(4k\pi)-3]$
O_9'	$\frac{2}{3}\cos(3k\pi)^2[9+5\cos(2k\pi)+4\cos(4k\pi)]$
O_{10}	$16\cos(k\pi)^2$
	$n=10$
O_1	$20\cos(k\pi)^2$
O_2	$5[1+\cos(4k\pi)]$
O_3	$-\frac{20}{3}\cos(3k\pi)^2[2\cos(4k\pi)-3]$
O_{4a}	$\frac{8}{25}(\Sigma_{n=0}^{9}\cos[(2n+1)k\pi])^2$
O_{4b}	$\frac{16}{5}\cos(k\pi)^2$
O_{4c}	$1+\frac{4}{5}\cos(2k\pi)$
O_{4d}	$\frac{4}{5}\cos(k\pi)^2$
O_5	$20\sin(k\pi)^2$
O_6	$\frac{4}{5}\cos(k\pi)^2$
O_7	$\frac{10}{3}[\cos(3k\pi)+\cos(9k\pi)]^2$
O_8	$-\frac{20}{3}\cos(3k\pi)^2[2\cos(4k\pi)-3]$
O_9'	$\frac{4}{15}\cos(3k\pi)^2[27+12\cos(2k\pi)+10\cos(4k\pi)]$
O_{10}	$20\cos(k\pi)^2$
	$n=9$
O_1	$18\cos(k\pi)^2$
O_{2a}	$\frac{2}{9}\cos(2k\pi)^2[41+9\cos(2k\pi)]$
O_{2b}	$\frac{1}{18}[82+9\cos(2k\pi)+80\cos(4k\pi)-9\cos(6k\pi)]$
O_{2c}	$-\frac{2}{9}\cos(2k\pi)^2[9\cos(2k\pi)-41]$
O_3	$-6\cos(3k\pi)^2[2\cos(4k\pi)-3]$
O_4	$1+\cos(2k\pi)$
O_{5a}	$\frac{4}{9}\cos(3k\pi)^2$
O_{5b}	$-\frac{1}{405}(1+\Sigma_{n=1}^{4}\cos(10nk\pi))^2[8\cos(2k\pi)-2\cos(4k\pi)$ $-8\cos(6k\pi)\quad+6\cos(8k\pi)-13]$
O_{5c}	$\frac{1}{27}[1-2\cos(2k\pi)]^2[83+18\cos(2k\pi)-18\cos(4k\pi)$ $-81\cos(6k\pi)]$
O_{5d}	$\frac{49}{36}(\Sigma_{n=0}^{7}(-1)^n\sin[(2n+1)k\pi])^2$
O_{5e}	$\frac{4}{81}\cos(2k\pi)^2\sin(k\pi)(1+2\Sigma_{n=1}^{4}\cos(8nk\pi))$
O_{5f}	$\frac{2}{81}(1+2\Sigma_{n=1}^{4}\cos(2nk\pi))^2$
O_{5g}	$-\frac{2}{9}\cos(2k\pi)^2[63\cos(2k\pi)-65]$
O_{6a}	$\frac{2}{9}\cos(k\pi)^2$
O_{6b}	$\frac{2}{81}[5+3\cos(2k\pi)](\Sigma_{n=0}^{8}\cos[(4n+2)k\pi])^2$
O_7	$-\frac{1}{3}[3\cos(2k\pi)-5][1+2\cos(4k\pi)]^2$
O_8'	$\frac{2}{3}(\Sigma_{n=0}^{2}\cos[(2n+1)k\pi])^2$
O_9	$\frac{2}{5}\cos(5k\pi)^2[21+8\cos(2k\pi)+10\cos(4k\pi)+16\cos(6k\pi)$ $-6\cos(8k\pi)]$
O_{10}	$18\cos(k\pi)^2$

structures of the different phases are shown in Fig. 5 and the others are constructed using the same repeating structure units as those in Fig. 2. There are two different ground states O_{6a} $(\theta=1/2)$ and O_{6b} $(\theta=5/12)$ derived from the O_6^G $(\theta=2/5)$ phase of dimer adsorbates on the graphite. The O_{6a} $(\theta=1/2)$ phase is a helical structure and the helical direction of the O_{6a} $(\theta=1/2)$ phase and the axis of the (8,0) nanotube form an angle α with $\tan\alpha=\sqrt{3}$. The O_{6b} $(\theta=5/12)$ phase is also a helical structure along the nanotube with $\tan\alpha=\sqrt{3}/9$. The translational generators of the two phases are both screw-axis translations, $(C_8^3|\frac{1}{8})$ for the O_{6a} $(\theta=1/2)$ phase and $(C_{16}^1|\frac{1}{16})$ for the O_{6b} $(\theta=5/12)$ phase. The O_4^G $(\theta=2/3)$ phase is split into two phases O_{4a} $(\theta=11/16)$ and O_{4b} $(\theta=5/8)$ due to the confinement in the rolling direction. However, the translational generators are not similar. For the O_{4a} $(\theta=11/16)$ phase it is pure translation $(E|1)$, while for the O_{4b} $(\theta=5/8)$ it is screw-axis translation $(C_{16}^3|\frac{1}{2})$. The O_7 $(\theta=1/3)$ phase is composed of rotated

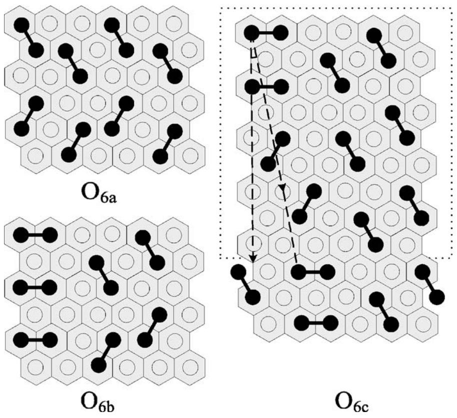

FIG. 3. Ground-state structures on the (6,0) nanotube. The structure in the dashed rectangle is the repeating helical unit of the O_{6c} phase. The axis direction of the nanotube and the helical direction of the repeating helical units are also shown.

basic structures, which has a $\left(C_{16}^{3}\middle|\frac{1}{4}\right)$ translational generator and keeps the C_4 symmetry of the (8,0) nanotube. Similar to the O_9' (θ=6/21) phase on the (7,0) nanotube, the O_9' (θ=1/4) phase is derived from the corresponding O_9^G (θ=4/15) phases with variation due to the confinement in the rolling direction. The structure of O_7 (θ=1/3) is kept on the (8,0) nanotube by rotation of the basic substructure and the line group is $L16_{12}22$ with the translational generator $\left(C_{16}^{3}\middle|\frac{1}{4}\right)$.

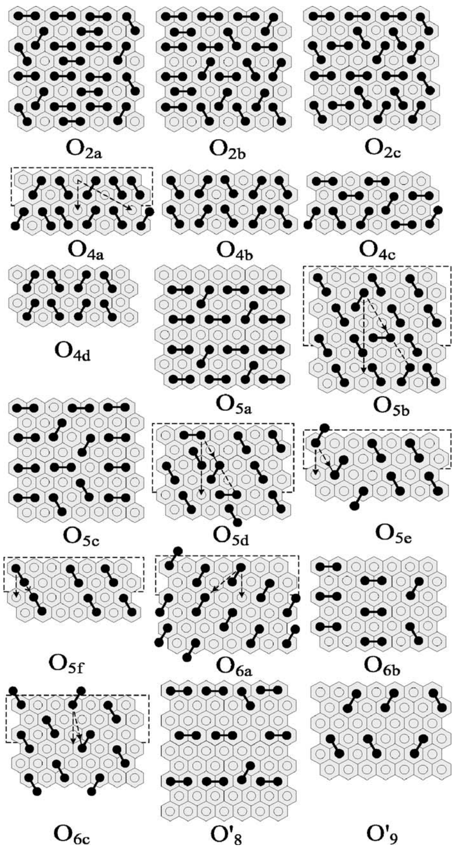

FIG. 4. Ground-state structures on the (7,0) nanotube. The structures in the dashed rectangles are the repeating helical units of the corresponding phases. The axis direction of the nanotube and the helical direction of the repeating helical units are also shown.

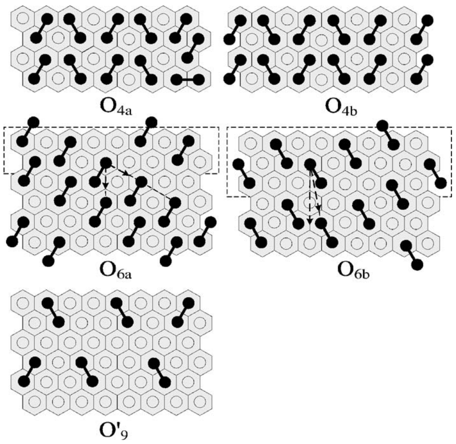

FIG. 5. Ground-state structures on the (8,0) nanotube. The structures in the dashed rectangles are the repeating helical units of the corresponding phases. The axis direction of the nanotube and the helical direction of the repeating helical units are also shown.

In the case of n=9, there are 19 ground states of dimer adsorbates. The phase diagram is shown in Fig. 1(e). The structures of the different phases are shown in Fig. 6 and the others are constructed using the same repeating structure units as those in Fig. 2. For the (9,0) nanotube, the O_6^G (θ=2/5) phase is split into two phases O_{6a} (θ=4/9) and O_{6b} (θ=7/18). The O_{6a} (θ=4/9) phase has the basic substructure of the O_6^G (θ=2/5) phase as the main part and the O_{6b} (θ=7/18) phase is a helical structure along the nanotube with tan $\alpha=\sqrt{3}/9$. Therefore the translational generator of the O_{6a} (θ=4/9) phase is $(E|1)$, while it is $\left(C_{9}^{1}\middle|\frac{1}{9}\right)$ for

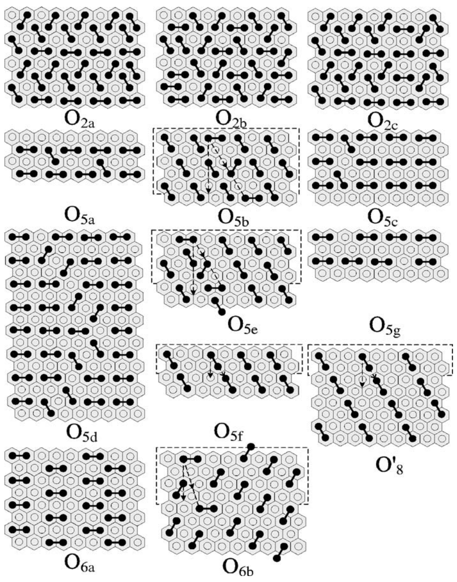

FIG. 6. Ground-state structures on the (9,0) nanotube. The structures in the dashed rectangles are the repeating helical units of the corresponding phases. The axis direction of the nanotube and the helical direction of the repeating helical units are also shown.

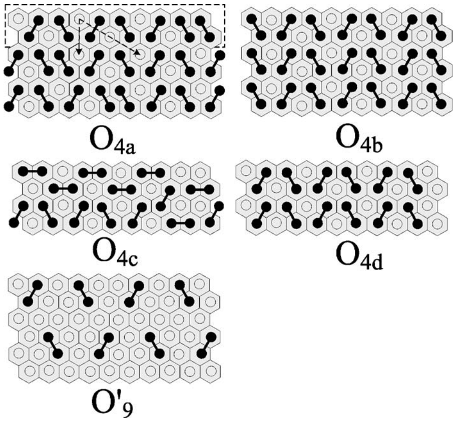

FIG. 7. Ground-state structures on the (10,0) nanotube. The structure in the dashed rectangle is the repeating helical unit of the corresponding phase. The axis direction of the nanotube and the helical direction of the repeating helical units are also shown.

the O_{6b} (θ=7/18) phase. The O_2^G (θ=3/4) phase is split into three phases O_{2a} (θ=7/9), O_{2b} (θ=3/4), and O_{2c} (θ=13/18) due to the confinement in the rolling direction. The O_5^G (θ=1/2) phase is split into seven phases O_{5a} (θ=5/9), O_{5b} (θ=8/15), O_{5c} (θ=14/27), O_{5d} (θ=1/2), O_{5e} (θ=1/2), O_{5f} (θ=4/9), and O_{5g} (θ=4/9). The O_{5b} (θ=8/15), O_{5e} (θ=1/2), and O_{5f} (θ=4/9) phases are helical structures. The helical directions of these three phases and the axis of the (9,0) nanotube have the same angle α with $\tan\alpha=\sqrt{3}/3$. But the translational generators of these three phases are not the same. They are $(C_{18}^{5}|\frac{1}{18})$, $(C_{9}^{2}|\frac{1}{9})$, and $(C_{18}^{1}|\frac{1}{18})$, respectively. For the O'_8 (θ=1/3) phase on the (9,0) nanotube, the basic substructure of the O_8^G (θ=1/3) phase is arranged obliquely to match the confinement in the rolling direction and keep the C_3 symmetry of the (9,0) nanotube.

In the case of n=10, there are 13 ground states of dimer adsorbates. The phase diagram is shown in Fig. 1(f). The structures of the different phases are shown in Fig. 7 and the others are constructed by the same repeating structure units as those in Fig. 2. On the (10,0) nanotube, the O_4^G (θ=2/3) phase is split into four phases O_{4a} (θ=7/10), O_{4b} (θ=7/10), O_{4c} (θ=13/20), and O_{4d} (θ=3/5). The structures of the O_{4b} (θ=7/10), O_{4c} (θ=13/20), and O_{4d} (θ=3/5) phases are derived from the O_4^G (θ=2/3) phase due to the confinement in the rolling direction. The vacancies of the O_{4a} (θ=7/10) phase form a helical line surrounding the nanotube. The helical line and the axis of the (10,0) nanotube form an angle α with $\tan\alpha=\sqrt{3}$ and the line group is $L20_7 2$ with the translational generator $(C_{20}^{3}|\frac{1}{20})$. The structure of the O'_9 (θ=4/15) phase is derived from the O_9^G (θ=4/15) phase.

Comparing the ground-state structures of dimer adsorbates with those of single-site adsorption on the graphite,[28] we find that for the high-coverage ground states with $\theta>1/2$, when we consider the ordered structures formed by vacancies, the structures have similar features with those of the single-site adsorption. For dimer adsorption on graphite, the vacancy structure of the O_2^G (θ=3/4) phase is the same as the 2×2 ordered structure of single-site adsorption. The vacancy structure of the O_3^G (θ=2/3) phase is the same as the 3×1 ordered structure of single-site adsorption. The vacancy structure of the O_4^G (θ=2/3) phase is the same as the $\sqrt{3}\times\sqrt{3}$ ordered structure of single-site adsorption. For dimer adsorption on (n,0) nanotubes, the vacancy structures of the O_{2i} phases, the O_{4i} phases, and the O_3 phase are similar to those of single-site adsorption.[28] The vacancies always form 3×1 ordered structures for the O_3 phase with increase of nanotube size n. The vacancies of the O_{4i} phases form ordered structures which can be derived from the $\sqrt{3}\times\sqrt{3}$ ordered structure of single-site adsorption with confinement in the rolling direction of the nanotubes. Also, the vacancy structures of the O_{2i} phases are similar to the ordered structures derived from the 2×2 ordered structure.

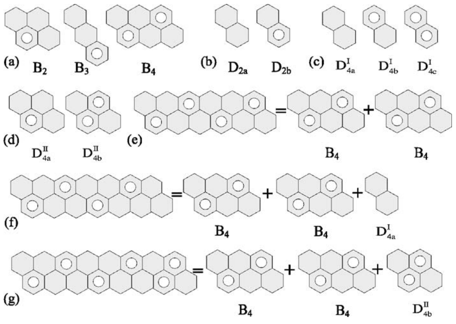

FIG. 8. (a) Vacancy basic substructures of the O_{2i}, O_3, and O_{4i} phases. The white circles represent vacancies. (b) Vacancy-derived substructures of the O_{2i} phases in the case of $n=2k+1$. (c) Vacancy-derived substructures of the O_{4i} phases in the case of $n=3k+1$. (d) Vacancy-derived substructures of the O_{4i} phases in the case of $n=3k+2$. (e) Representation of the vacancy-ordered structure of the O_4 phase by two B_4 vacancy basic substructures in the case of n=6. (f) Representation of the vacancy-ordered structure of the O_{4b} phase by two B_4 vacancy basic substructures and one vacancy-derived substructure D^I_{4a} in the case of n=7. (g) Representation of the vacancy-ordered structure of the O_{4b} phase by two B_4 vacancy basic substructures and one vacancy-derived substructure D^{II}_{4b} in the case of n=8.

In the following, we discuss in detail the variation tendency of the vacancy structures of the high-coverage phases on the nanotubes with increase of nanotube size n. We first consider the O_{4i} phases as an example. There are three sites along the rolling direction of the (n,0) nanotubes in the primitive cell of the complementary vacancy structure of the O_4^G (θ=2/3) phase on graphite. The primitive cell of the vacancy structure can be used as the vacancy basic substructure to construct the vacancy ordered structures of the O_{4i} phases on nanotubes. Figure 8(a) shows the vacancy basic substructures of the O_{2i}, O_3, and O_{4i} phases. When n=6, which can be divided by the site number (3) of the vacancy basic substructure B_4 along the rolling direction, the vacancy structure of the O_4 (θ=2/3) phase for the (6,0) nanotube is the same as that of the O_4^G phase. The primitive cell of the vacancy structure of the O_4 (θ=2/3) phase is composed of two B_4 vacancy basic substructures, as shown in Fig. 8(e). The line group is $L4_2/mcm$ for the O_4 (θ=2/3) phase in the case of n=6. When n=7, which cannot be divided by 3, the O_4 phase is split into four different phases. The O_{4a} ($\theta=5/7$) phase has helical structure, which can be seen as formed by the screw-axis rotation of the primitive cell of the O_{4b} ($\theta=5/7$) phase by $6\pi/14$ around the nanotube axis and then translation by two lattice sites. The line group of O_{4a} ($\theta=5/7$) is $L14_52$, and the translational generator is $\left(C_{14}^3\middle|\frac{1}{14}\right)$. As is shown in Fig. 8(f), the primitive cell of the vacancy structure of the O_{4b} ($\theta=5/7$) phase is composed of two B_4 vacancy basic substructures and one vacant (occupied by adsorbed dimers) vacancy-derived substructure D_{4a}^I. Similarly, the primitive cell of the vacancy structure of the O_{4c} ($\theta=9/14$) phase is composed of two B_4 vacancy basic substructures and one half-full vacancy-derived substructure D_{4b}^I. The primitive cell of the vacancy structure of the O_{4d} ($\theta=4/7$) phase is composed of two B_4 vacancy basic substructures and one full vacancy-derived substructure D_{4c}^I. The line groups are $L\bar{2}2c$ for the O_{4b} ($\theta=5/7$) phase and $L\bar{2}2m$ for the other two phases. In case of $n=8$, the O_4 phase is split into two ground states, the O_{4a} ($\theta=11/16$) and O_{4b} ($\theta=5/8$) phases. The primitive cell of the vacancy structure of the O_{4a} ($\theta=11/16$) phase is composed of two B_4 vacancy basic substructures and one vacancy-derived substructure D_{4a}^{II}. The primitive cell of the vacancy structure of the O_{4b} ($\theta=5/8$) phase is composed of two B_4 vacancy basic substructures and one half-full vacancy-derived substructure D_{4b}^{II}, which is shown in Fig. 8(g). The line groups are $L\bar{1}m$ for the O_{4a} ($\theta=11/16$) phase and $L16_82$ for the O_{4b} ($\theta=5/8$) phase. When $n=9$, which can be divided by 3 again, the O_4 phase remains unchanged and the line group is $L6_3/\mathrm{mcm}$, which belongs to the same line group family[37] as for the case $n=6$. The primitive cell of the vacancy structure of the O_4 phase is composed of three repeated B_4 vacancy basic substructures. In the case of $n=10$, the O_4 phase is split into four new ground states again. The derived substructures of the O_{4i} phases are the same as those of $n=7$. The line group of the O_{4a} ($\theta=7/10$) phase is $L20_72$, belonging to the same line group family as for the case $n=7$, and the translational generator is $\left(C_{20}^3\middle|\frac{1}{20}\right)$. The line groups of the O_{4i} ($i=b,c,d$) phases are the same as those of the corresponding phases on the (7,0) nanotube. The only difference between the cases $n=10$ and $n=7$ is the repeated unit numbers of the vacancy basic substructure B_4, increased from two to three.

Similar to the case of single-site adsorption, in order to maintain the lowest energy for the ground states, the ground-state structures should contain as many vacancy basic substructures as possible. The vacancy basic substructures of the O_4 phase have three sites along the rolling direction of $(n,0)$ nanotubes. Thus the variation periodicity of the O_4 phase with increase of n is 3, which is the same as that of the $\sqrt{3}\times\sqrt{3}$ ordered structure of single-site adsorption. We have also calculated dimer adsorbates with large nanotube size n, and the results confirm the above variation tendency. However, the vacancy arrangements in the derived substructures are different from those of the ordered structures of single-site adsorption, because one dimer occupies two neighboring sites. Although the vacancy structures of the O_{4i} phases do not correspond to those ordered structures of the single-site adsorption one by one, the variation periodicities of both cases are the same with increase of nanotube size n.

TABLE III. Coverage θ and line group of the high-coverage O_{2i}, O_3, and O_{4i} phases on $(n,0)$ nanotubes.

n	Phase No.	Coverage	Line group
$2k$	O_2	$\frac{3}{4}$	$L(2k)_k/mcm$
$2k+1$	O_{2a}	$\frac{3k+2}{4k+2}$	$L\bar{2}2c$
	O_{2b}	$\frac{6k+3}{8k+4}$	$L\bar{2}2m$
	O_{2c}	$\frac{3k+1}{4k+2}$	$L\bar{2}2c$
Any	O_3	$\frac{2}{3}$	$L(2n)_n/mcm$
$3k$	O_4	$\frac{2}{3}$	$L(2k)_k/mcm$
$3k+1$	O_{4a}	$\frac{2k}{3k+1}$	$L(6k+2)_{(2k+1)}2$
	O_{4b}	$\frac{2k}{3k+1}$	$L\bar{2}2c$
	O_{4c}	$\frac{4k+1}{6k+2}$	$L\bar{2}2m$
	O_{4d}	$\frac{2k+1}{3k+1}$	$L\bar{2}2c$
$3k+2$	O_{4a}	$\frac{2k+1}{3k+2}$	$L\bar{1}m$
	O_{4b}	$\frac{4k+3}{6k+4}$	$L(2n)_n2$

The variation periodicity of the O_{2i} phases with increase of nanotube size n is 2 because the vacancy basic substructure of the O_{2i} phases is the same as the corresponding 2×2 ordered structure of single-site adsorption. We can obtain the relation of the coverage θ and line groups of the high-coverage O_{2i}, O_3, and O_{4i} phases with nanotube size n as shown in Table III. Figure 9 shows the coverage as a function of nanotube size n.

When we consider the dimer arrangements, the O_1^G, O_2^G, O_3^G, and O_4^G phases of dimer adsorbates on graphite are highly degenerate. However, those degenerate structures for each phase have the same vacancy structure. When the coverage $\theta=1$, the number of different dimer coverings on the triangular lattice with $M\times N$ sites has been found by Fendley *et al.* and even on a 6×4 triangular lattice there are 749 types of dimer coverings.[43] The orientation of dimers leads to variety of dimer coverings in the high-coverage ground states and causes the structures for dimer adsorption to be more complex as compared with those for single-site adsorption. The vacancy structures in these high-coverage ground states are ordered and nondegenerate. The vacancy structures

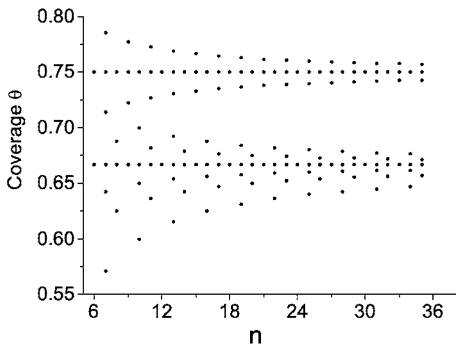

FIG. 9. Variation of the coverage as a function of n.

can show the ordering and coverage of dimer adsorbates, but lose the degeneracy of dimer coverings. Since the vacancy-ordered structures of the O_2^G, the O_3^G, and the O_4^G phases are the same as those of single-site adsorption, the variation periodicities of the O_{2i} phases, the O_{4i} phases, and the O_3 phase with increase of nanotube size n are the same as those of single-site adsorption.

For the low coverage phases of dimer adsorption with coverage $\theta \leqslant 1/2$, there are no degenerate structures due to dimer orientation. Thus we described the ordered structures directly by the arrangements of the adsorbed dimers. The structures and variation tendency of the ground states of both the dimer and vacancy configurations are different from those of single-site adsorption. We analyze the variation tendency of the O_{6i} phases as an example. In the case of $n=6-9$, the structures of the O_{6i} phases cannot be simply constructed using the basic substructure (the primitive cell of the O_6^G phase) plus the derived substructures and the symmetries of corresponding O_{6i} phases do not belong to the same line group family.[37] for $n=10$, which is twice the site number of the primitive cell of the O_6^G ($\theta=2/5$) phase in the rolling direction, the repeating structure of the O_6 ($\theta=2/5$) phase on the (10,0) nanotube is composed of two basic substructures. The primitive cell of the O_5^G ($\theta=1/2$) phase has two sites along the rolling direction. In the case of $n=7$, the O_5^G ($\theta=1/2$) phase is split into six phases, while in the case of $n=9$, it is split into seven phases. Comparing the two cases, there are four similar ground-state structures. However, the O_{5e} ($\theta=3/7, n=7$) phase, which is a helical structure on the (7,0) nanotube, does not have the corresponding structure on the (9,0) nanotube. The O_{5c} ($\theta=14/27, n=9$) and O_{5g} ($\theta=4/9$, $n=9$) phases on the (9,0) nanotube do not have corresponding structures on the (7,0) nanotube. In contrast to the O_{5e} ($\theta=3/7, n=7$) phase, the O_{5c} ($\theta=14/27, n=9$) and O_{5g} ($\theta=4/9, n=9$) phases do not have helical structures. They are more similar to the O_5^G ($\theta=1/2$) phase on graphite, consistent with the fact that the $(n,0)$ nanotubes are more like graphite sheets when the nanotube size n increases.

For the low-coverage phases of dimer adsorption, if the nanotube size n is compatible with the basic substructures, the symmetries of the corresponding phases are similar. Although the O_7 phase disappears in the case of $n=7$ due to confinement, it can be seen from Table I that the line groups of the O_7 phases on the other $(n,0)$ nanotube belong to the same line group family.[37] When n is not a multiple of the site number of the primitive cells of the O_i^G phases in the rolling direction, the adsorbed dimers may form helical structures on the nanotube for those ground states with low coverage. An obvious example is the O_8' ($\theta=1/3$) phase on the (9,0) nanotube. The primitive cell of the O_8^G ($\theta=1/3$) phase has two sites in the rolling direction. When $n=9$, for the O_8' ($\theta=1/3$) ground-state phase, the basic substructure becomes an oblique structure to match the confinement along the rolling direction. Therefore the line group of the O_8' ($\theta=1/3, n=9$) phase is $L18_32$, not belonging to the same line group family as for the case $n=2k$. When the next-nearest-neighbor interaction J_2 and the chemical potential μ are in a certain range, as in the phase area of O_4^G ($\theta=2/5$) or O_6^G ($\theta=1/2$), the basic substructures are rotated to provide a larger space for adsorbed dimers and to reduce the energy of the adsorbate structure. Thus helical structures are formed on the $(n,0)$ nanotube. For single-site adsorption, a vacant site can always be occupied by an adsorbed atom. In dimer adsorption, an isolated vacant site cannot be occupied, and we need two neighboring vacant sites for occupation by a dimer. This leads to a difference between dimer adsorption and single-site adsorption, and makes the structures and the phase diagrams of the dimer adsorption more complex.

IV. SUMMARY

We have studied the adsorption of diatomic molecules on graphite sheets and on nanotubes. The adsorption of diatomic molecules can be described as the adsorption of dimers on a triangular lattice. Using Monte Carlo simulation, we have determined the ground states for dimer adsorption. The ground-state phase diagrams of dimer adsorbates on graphite and on $(n,0)$ nanotubes have been obtained. The symmetries of adsorbate structures on the $(n,0)$ nanotube are described using the line group method.

We find that for the ground states of the dimer adsorption with high coverage ($\theta > 1/2$), the vacancy structures of the ground states are similar to the ordered structures of single-site adsorption. We have obtained the variation periodicities of the high-coverage phases with increase of nanotube size n. By this variation tendency, we show how the high-coverage ground states on the $(n,0)$ nanotube approach the corresponding ground states on graphite as the nanotube size n increases.

For the ground states of dimer adsorption with coverage $\theta \leqslant 1/2$, the structures are different from those of single-site adsorption and more complex. Since a dimer needs to occupy two neighboring lattice sites, helical structures are formed for the dimer adsorption on $(n,0)$ nanotubes due to the confinement of nanotubes when the site number does not match that of the basic substructure along the rolling direction.

ACKNOWLEDGMENTS

This research was supported by the National Natural Science Foundation of China under Grant No. 10474049 and the National Basic Research Program of China.

[1] J. Zhao, A. Buldum, J. Han, and J. P. Lu, Nanotechnology **13**, 195 (2002).

[2] M. Arab, F. H. Picaud, M. J.-P. Devel, C. Ramseyer, and C. Girardet, Phys. Rev. B **69**, 165401 (2004).

[3] M. M. Calbi, M. W. Cole, S. M. Gatica, M. J. Bojan, and G. Stan, Rev. Mod. Phys. **73**, 857 (2001).

[4] X. Y. Zhu, S. M. Lee, Y. H. Lee, and T. Frauenheim, Phys. Rev. Lett. **85**, 2757 (2000).

[5] K. Tada, S. Furuya, and K. Watanabe, Phys. Rev. B **63**, 155405 (2001).

[6] A. Kleinhammes, S. H. Mao, X. J. Yang, X. P. Tang, H. Shimoda, J. P. Lu, O. Zhou, and Y. Wu, Phys. Rev. B **68**, 075418 (2003).

[7] S. Santucci, S. Picozzi, F. Di Gregorio, L. Lozzi, C. Cantalini, L. Valentini, J. M. Kenny, and B. Delley, J. Chem. Phys. **119**, 10904 (2003).

[8] O. Byl, P. Kondratyuk, S. T. Fouth, S. A. FitzGerald, L. Chen, J. K. Johnson, and J. T. Yates, Jr., J. Am. Chem. Soc. **125**, 5889 (2003).

[9] W. Shi and J. K. Johnson, Phys. Rev. Lett. **91**, 015504 (2003).

[10] G. Q. Ning, F. Wei, G. H. Luo, Q. X. Wang, Y. L. Wu, and H. Yu, Appl. Phys. A: Mater. Sci. Process. **78**, 955 (2004).

[11] L. Firlej and B. Kuchta, J. Low Temp. Phys. **139**, 599 (2005).

[12] A. Tchernatinsky, S. Desai, G. U. Sumansekera, C. S. Jayanthi, S. Y. Wu, B. Nagabhirava, and B. Alphenaar, J. Appl. Phys. **99**, 034306 (2006).

[13] P. G. Collins, K. Bradley, M. Ishigami, and A. Zettl, Science **287**, 1801 (2000).

[14] A. Modi, N. Koratkar, E. Lass, B. Wei, and P. M. Ajayan, Nature (London) **424**, 171 (2003).

[15] X. Yang and J. Ni, Phys. Rev. B **71**, 165438 (2005).

[16] S. Guerini, A. G. Souza Filho, J. M. Filho, O. L. Alves, and S. B. Fagan, Phys. Rev. B **72**, 233401 (2005).

[17] G. Gundiah, A. Govindaraj, N. Rajalakshmi, K. S. Dhathathreyan, and C. N. R. Rao, J. Mater. Chem. **13**, 209 (2003).

[18] I. Cabria, M. J. López, and J. A. Alonso, J. Chem. Phys. **123**, 204721 (2005).

[19] N. Hu, X. Sun, and A. Hsu, J. Chem. Phys. **123**, 044708 (2005).

[20] S. Dag, Y. Ozturk, S. Ciraci, and T. Yildirim, Phys. Rev. B **72**, 155404 (2005).

[21] G. Vidali, G. Ihm, H. Y. Kim, and M. W. Cole, Surf. Sci. Rep. **12**, 133 (1991).

[22] M. Caragiu and S. Finberg, J. Phys.: Condens. Matter **17**, R995 (2005).

[23] M. S. Dresselhaus and G. Dresselhauls, Adv. Phys. **51**, 1 (2002).

[24] E. Durgun, S. Dag, V. M. K. Bagci, O. Gülseren, T. Yildirim, and S. Ciraci, Phys. Rev. B **67**, 201401(R) (2003).

[25] B. Mihura and D. P. Laudan, Phys. Rev. Lett. **38**, 977 (1977).

[26] U. Brandt and J. Stolze, Z. Phys. B: Condens. Matter **64**, 481 (1986).

[27] M. Kaburagi and J. Kanamori, Jpn. J. Appl. Phys., Suppl. **2**, 145 (1974).

[28] X. Yang and J. Ni, Phys. Rev. B **67**, 195403 (2003).

[29] S. M. Heald and E. A. Stern, Phys. Rev. B **17**, 4069 (1978).

[30] S. H. Jhi, S. G. Louie, and M. L. Cohen, Solid State Commun. **123**, 495 (2002).

[31] J. E. González, A. J. Ramirez-Pastor, and V. D. Pereyra, Langmuir **17**, 6974 (2001).

[32] A. J. Ramirez-Pastor, J. L. Riccardo, and V. D. Pereyra, Surf. Sci. **411**, 294 (1998).

[33] W. Rżysko and M. Borówko, J. Chem. Phys. **117**, 4526 (2002).

[34] M. E. J. Newman and G. T. Barkema, *Monte Carlo Methods in Statistical Physics* (Clarendon Press, Oxford, 1999).

[35] C. R. A. Abreu, F. C. Peixoto, R. O. Corrêa, A. S. Telles, and F. W. Tavares, Braz. J. Chem. Eng. **18**, 385 (2001).

[36] M. Damnjanović, I. Milošević, T. Vuković, and R. Sredanović, Phys. Rev. B **60**, 2728 (1999).

[37] M. Damnjanović, T. Vuković, I. Milošević, and B. Nikolić, Acta Crystallogr., Sect. A: Found. Crystallogr. **57**, 304 (2001).

[38] M. Vujičić, I. B. Bozović, and F. Herbut, J. Phys. A **10**, 1271 (1977).

[39] S. C. Erwin and C. S. Hellberg, Surf. Sci. **585**, L171 (2005).

[40] W. Stephan and B. W. Southern, Phys. Rev. B **61**, 11514 (2000).

[41] E. Rastelli, S. Regina, and A. Tassi, Phys. Rev. B **73**, 144418 (2006).

[42] R. Saito, G. Dresselhaus, and M. S. Dresselhaus, *Physical Properies of Carbon Nanotubes* (Imperial College Press, London, 1998).

[43] P. Fendley, R. Moessner, and S. L. Sondhi, Phys. Rev. B **66**, 214513 (2002).